Ferroelectricity in metal-organic frameworks: characterization and mechanisms

Asadi, Kamal; van der Veen, Monique

DOI
10.1002/ejic.201600932

Publication date
2016

Document Version
Accepted author manuscript

Published in
European Journal of Inorganic Chemistry

Ferroelectricity in metal-organic frameworks: characterization and mechanisms

Kamal Asadi,*[1] Monique Ann van der Veen*[2]

Abstract: Ferroelectric metal organic frameworks are emerging as an exciting field of research, and have witnessed a great progress in the last decade. In this contribution we briefly discuss ferroelectricity and its means of demonstration. We critically discuss different mechanisms leading to ferroelectricity as well as the state-of-the-art ferroelectric metal-organic frameworks.

1. Introduction

Metal-organic frameworks (MOFs) are composed of small metallic clusters linked by molecular linkers in an orderly manner. Depending on the coordination of the metal and the type of organic ligand used, different but well-defined three dimensional crystalline porous structures can be built.[1] MOFs' primary envisioned applications include gas storage, sorption, chemical sensing,[2] carbon capture and catalysis.[3]

Their inherent flexibility in the design, enables integration of different functionalities into the framework by employing different constituents. Lanthanides have been extensively used in fabrication of highly luminescent MOFs.[4,5] Magnetic MOFs have been demonstrated by incorporation of metallic clusters that contain elements like Mn.[6] Observation of semiconducting behavior has raised the expectations for MOF application in electronic devices and electrocatalysis.[7-9] Ferroelectric MOFs, wherein the crystalline structure is polar and its polarity can be reversibly switched by an external electric field (see Figure 1), form another important subcategory of the functional MOFs.

Ferroelectricity was first discovered in Rochelle salt by Valasek in 1920.[10] Rochelle salt is considered as a predecessor of metal-organic frameworks. Since its discovery, ferroelectricity has been observed in different materials ranging from ceramics[11] to polymers,[12-14] molecular crystals[15,16] and organic-inorganic hybrid materials.[17,18]

Ferroelectrics are technologically interesting materials with diverse applications in areas like data storage, (ultrasound) sensing and actuation, energy harvesting and opto-electronics. Ceramics followed by polymers are the two frontrunners of integrated ferroelectrics.[19] Emerging ferroelectric materials as metal-organic frameworks are still in the fundamental research phase, and application is not yet in horizon.

Although ferroelectricity appears to be a niche research focus in the MOF field, in the last ten years gradually more papers concerning ferroelectric MOFs have been published. The developments in field of ferroelectric MOFs until 2012 has already been extensively reviewed.[20-22] In this review, we discuss new developments since 2012. We note that the paper does not serve as a comprehensive review but rather reflects our personal perspective on the topic. We will briefly discuss ferroelectricity, and present an overview of the structural-physical characterization techniques. With the insight gained on measurement methods and data interpretations, we then critically assess the latest developments and discuss the proposed mechanisms for ferroelectricity in MOFs. We present a protocol for device fabrication and measurement method and finally end with an outlook for ferroelectric MOF research.

[1] K., Asadi
Humboldt Research Group
Max-Planck Insititute for Polymer Research
Ackermannweg 10, 55128 Mainz, Germany
E-mail: asadi@mpip-mainz.mpg.de
http://www.mpip-mainz.mpg.de/4076382/Humboldt_Research_Group_Asadi

[2] M.A., van der Veen
Catalysis Engineering, Department of Chemical Engineering
Delft University of Technology
Van der Maasweg 9, 2629HZ Delft, the Netherlands
E-mail:m.a.vanderveen@tudelft.nl
http://cheme.nl/ce/people/monique-van-der-veen/

Monique A. obtained her PhD in 2010 at the University of Leuven in the groups of Dirk De Vos and Thierry Verbiest for pioneering the use of nonlinear optics to study the structure and dynamics of nanoporous host/guest materials. With a personal postdoctoral fellowship awarded by the Scientific Research Fund Vlaanderen (FWO) she continued to work at the University of Leuven, and at the Max-Planck Institute for Polymer Research in Mainz, Germany. In 2013 she joined the Catalysis Engineering group at TU Delft, the Netherlands, as assistant professor. Her research focusses on the development of nanoporous materials, most notably metal-organic frameworks, for use in photocatalysis and in electronics. She has published 25 peer-reviewed journal articles which have been cited more than 800 times.

Kamal Asadi Kamal Asadi received his PhD degree in solid-state physics from University of Groningen, the Netherlands in 2009. His PhD research work and patents contributed to the demonstration of the first organic ferroelectric memory array and its logic table. Following a Post-Doc period, he joined Royal Philips Electronics N.V. as a research scientist. His work at Philips was focused on the investigation of metal-oxides, ferroelectrics and graphene for opto-electronic applications. In 2013 he moved to Max-Planck Institute for Polymer Research as a senior scientist. In 2014 he was awarded the Sofja Kovalevskaja Award of the Alexander von Humboldt Foundation for his project on organic multi-ferroics. His research at the moment is focused on electronic devices based on organic/inorganic hybrids. He is co-author of numerous papers and holder of eight patents.

2. Ferroelectricity

2.1. Introduction

There are a number of books[23] and excellent reviews[24-27] dealing with ferroelectricity in different materials and the applications. Here we present a brief but essential introduction to ferroelectricity in materials. In what follows we discuss the different responses different types of insulating materials can show in response to an electrical field, starting with dielctric materials and ending with ferroelectric materials.

Electrical polarization: Dielectric materials polarize when placed in an external electric field, *E,* due to the alignment of small molecular dipoles with respect to the applied field. Dielectrics therefore show a spontaneous polarization, P_s, which disappears after field removal. For linear dielectrics, the electric displacement, *D*, varies linearly with *E* and a *D-E* plot therefore appears as a straight line passing through the origin. Schematic *D-E* plots for linear and non-linear dielectrics are shown in Figure 2a,b and 2c, d respectively.

Piezoelectricity: When the dielectric is crystalline and the unit cell is not centrosymmetric, a relatively large mechanical strain is induced that is proportional to the applied field *E*. Therefore under electrical stress, piezoelectric crystals deform and a macroscopic dipole appears (inverse piezoelectric effect). Polarization disappears after field removal. Piezoelectrics generate voltage while under mechanical stress (direct piezoelectric effect).

Pyroelectricity: Pyroelectrics are a subclass of the piezoelectric wherein the crystal possesses a unique polar axis and the material is polarized even in the absence of an external electric field.[28] Spontaneous polarization in pyroelectrics varies with temperature. At temperatures that are high enough, the crystal goes through a phase transition and spontaneous polarization disappears. Pyroelectrics therefore show a sharp peak in their pyroelectric current at the phase transition temperature.

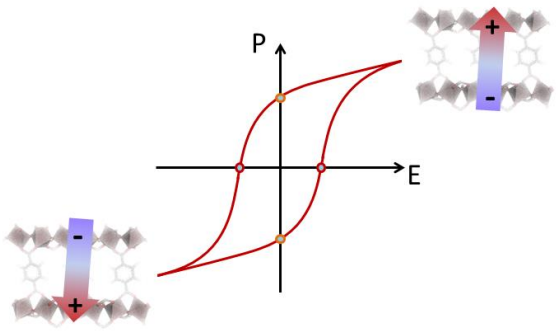

Figure 1. Schematic representation of the dependency of the polarization with applied electric field for ferroelectric metal-organic frameworks.

Ferroelectricity: Ferroelectrics are a subclass of pyroelectrics whose crystalline polarization can be reversed by an external electric field. Ferroelectrics therefore possess a permanent electric dipole in their crystalline unit cell whose direction can be switched with the external electric field *E*, resulting in a hysteretic behavior in their polarization response versus *E*, as shall be discussed below.

2.2. Identification of ferroelectricity

A schematic hysteretic *D-E* loop of a ferroelectric is shown in Figure 1e. Ferroelectrics show remnant polarization, P_r, which is defined as the polarization that is present in the material after the external field is removed. The coercive field E_c is defined as the field needed to set the polarization back to zero. Alternatively E_c can be defined as a threshold field at which the polarization switches sign. Values for P_s, P_r, and E_c are derived from the *D-E* plot.

A wide range of analytical techniques are required to properly analyze and claim ferroelectricity in a new material. Since the most common and straight forward method for demonstration of ferroelectricity is to measure hysteretic *D-E* loop using the so-called Sawyer-Tower circuit, the majority of the ferroelectric MOF literature focuses therefore on demonstration of the *D-E* loops. The dispute over ferroelectricity of a banana skin[29] has highlighted the extra care that should be taken in the interpretation of electrical polarization loops and the claim of ferroelectricity. Complimentary characterization techniques should be used to demonstrate ferroelectricity of a new material. Here a set of measurements techniques to assess ferroelectricity in MOFs is provided.

Structural analysis: The first and foremost crucial measurement is X-ray diffraction (XRD) to prove the non-centrosymmetric crystalline structure. Among 21 non-centrosymmetric crystalline classes 20 are piezoelectric among which 10 are also pyroelectrics. Centro-symmetric crystals possess a center of inversion symmetry meaning that within the crystal, there exists a point (center) with respect to which the inverted crystal is identical with the starting structure. The crystal classes and the corresponding crystalline structure of the pyroelectrics are given in the supporting information Table S1.

Since ferroelectrics are subclass of pyroelectrics, the crystalline structure of any new MOF compounds should fall into one of the mentioned crystalline structure in order to be considered as a “potential” ferroelectric material. It must be however noted that due to complicated chemical and geometrical structures, it is sometimes challenging to distinguish non-centrosymmetry in a MOF crystal. As a complement to XRD crystallographic analysis, optical spectroscopic techniques such as second harmonic generation (SHG) can be used.

Thermal properties: Ferroelectrics are all pyroelectrics. Therefore when the temperature of the compound varies, the spontaneous polarization of the crystal changes so that an excess of free charge appears which gives rise to the current flow in the crystal and external circuit. The experiment is

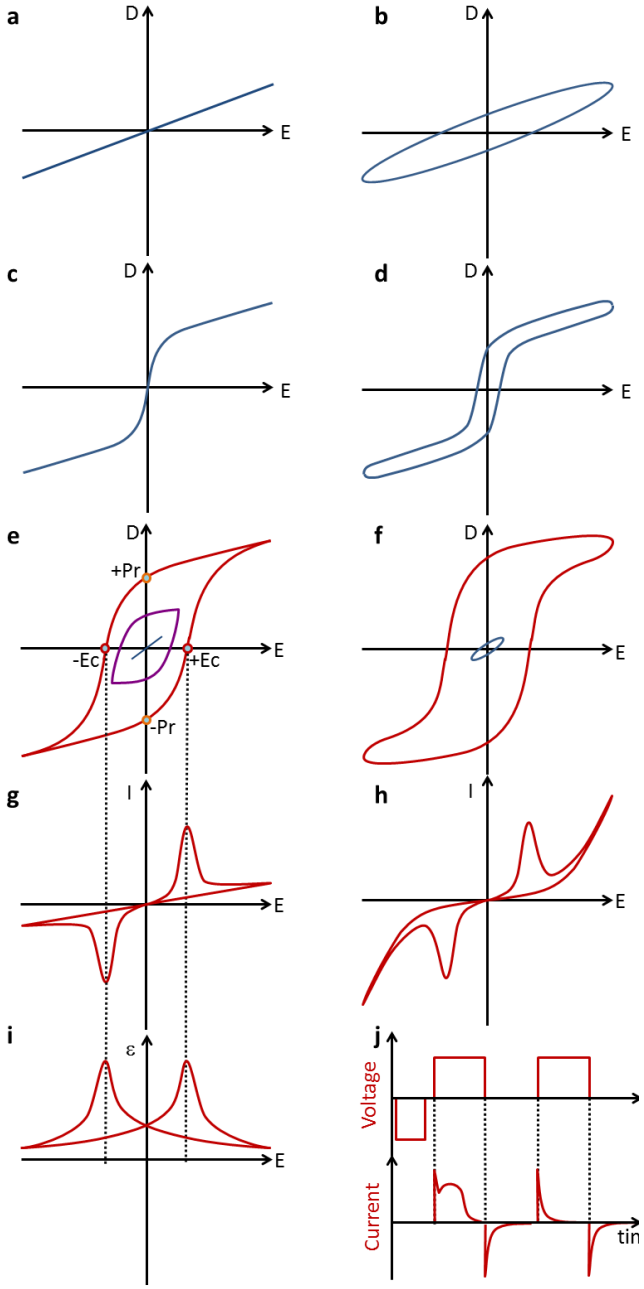

Figure 2. Schematic representation of displacement (or polarization) of a) an ideal linear dielectric b) a slightly conductive linear dielectric c) an ideal non-linear dielectrics d) a slightly conductive non-linear dielectric e) an ideal true ferroelectric with the inner loops at low and intermediate fields f) a slightly conductive ferroelectric with the inner loop at low fields g-h) shunt measurement of an ideal and non-ideal ferroelectric wherein switching peaks are clearly visible and its maxima coincides with coercive fields, i) the "Butterfly" dielectric response of a ferroelectric as function of applied electric field measured using small amplitude capacitance-voltage and j) is the response of a PUND measurement.

performed under constant electric field and constant elastic stress for an unclamped crystal *i.e.* a crystal that is completely free to expand or contract. The pyroelectric coefficient vector, p, is then defined as: $p = dP_S/dT$, where T is temperature in Kelvin. For ferroelectrics there exists a critical temperature, called Curie temperature T_c, above which the material goes through ferroelectric-paraelectric phase transition and the crystalline structure transforms into a high-temperature non-polar phase. At T_c the spontaneous polarization disappears as schematically shown in Figure 3a, and the pyroelectric current peaks, as shown in Figure 3b.

The most straight forward technique is to measure the pyroelectric dynamically, where the pyroelectric material is heated uniformly at a constant rate dT/dt of 1-2 K per minutes and the pyroelectric current is measured, Figure 3b. Different measurement methods are well described elsewhere.[30,31] Here we have intentionally excluded discussion on thermal methods based on electrocaloric effects, specific heat or high pressure studies which are suited for advanced pyroelectric characterizations.

Dielectric spectroscopy: Dielectric measurements are most commonly used for the identifications of phase transitions and recording of the transition temperatures. For frequencies below 100 MHz, small signal dielectric spectroscopy is used, where the sample is usually contacted with metallic electrodes. Dielectric constant and loss as a function of temperature are obtained from admittance measurements. Unclamped ferroelectrics show a large increase in their dielectric constant at the ferroelectric-paraelectric phase transition temperature as schematically shown in Figure 3c.

Phase transition affects the dielectric constant, ε, as the ferroelectrics shows an anomaly at T_c, Curie temperature, as shown schematically in Figure 3c, which is described by the Curie–Weiss law:

$$\frac{\varepsilon}{\varepsilon_0} = \frac{C}{T - T_C}$$

where ε_0 is the permittivity of vacuum, C is the Curie constant, and T_C is the Curie–Weiss temperature.

Second harmonic generation response (SHG): Ferroelectric materials are inherently excellent nonlinear optical materials due to the lack of center of inversion symmetry. The electric field of the incident light induces electronic polarization in the material. The induced dipole oscillates with the frequency of the incident light and reradiates an electric field according to Maxwell's equations. In general the polarization P is written as:

$$P(t) = P_0 + \varepsilon_0 \chi_e E(t) + \chi^{(2)} E(t)^2 + higher\ orders$$

where, P_0 is a constant time independent polarization, and χ is the electric susceptibility. The term containing second powers of the electric field E gives rise to second harmonic generation, that is responsible for doubling the frequency (or halving the wavelength) of the incident light.

Optical SHG is a sensitive non-contact technique tool for probing local polar order and structural symmetry in ferroelectric materials.[32] SHG further allows for *in-situ* study of dynamical effects such as phase transitions, as schematically shown in Figure 3d, the SHG response disappears at T_c. Furthermore SHG-microscopy also allows for the determination of the point group symmetry of the crystal, and can be used to complement XRD.[33]

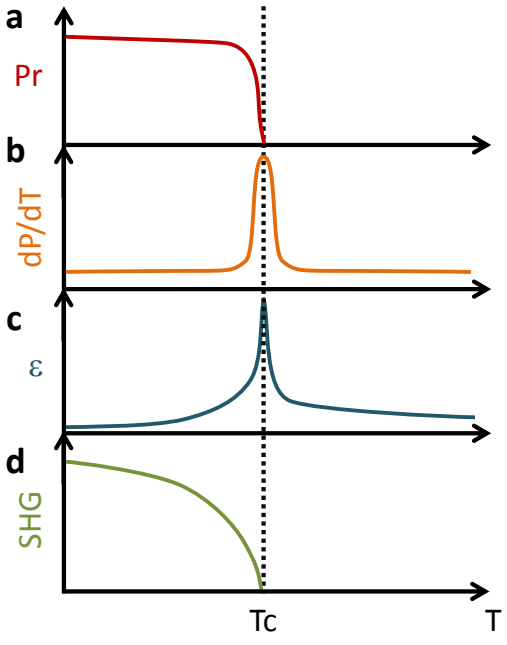

Figure 3. Schematic response of different physical properties of a ferroelectric material to temperature change: a) polarization drop of ferroelectric as a function of temperature due to its pyroelectricity b) pyroelectric current c) dielectric constant anomaly and d) SGH response. Note the change in response of different properties at Curie temperature, Tc.

Mechanical properties: Ferroelectrics are all good piezoelectrics due to the presence of polarization. Piezoelectrics can be characterized for their direct piezoelectric effect using methods such as "Berlincourt".[34] When the material is electrically contacted the inverse piezoelectric effect can be probed, where strain is then measured as a function of electric fields. The measurements methods for bulk and thin-film are well-established and reviewed in several books.[35]

Piezoelectric force microscopy (PFM): PFM is a scanning probe microscopy based technique that allows for manipulating of the domains and probing polarization dynamics at nanometer scale at high-resolutions. In PFM a conductive tip is in contact with the sample and an electrical voltage is applied between the tip and the bottom electrode.[36] Due to the inverse piezoelectric effect, the ferroelectric material responds with an expansion or contraction. The movement of the crystal is followed by the cantilever deflection. Applying an alternating bias, V_{AC}, results in an alternating deflection commonly referred as the PFM signal whose amplitude and phase contain information about the local piezoelectric strength and orientation of the ferroelectric domain.[37,38]

It has been shown that PFM hysteresis loops can also originate from a number of non-ferroelectric mechanisms.[39] Upon exclusion of the parasitic effects, PFM is a powerful technique for the study of switching and domain dynamics at the nanoscale.[39]

Electrical measurements: The most common method for demonstration of ferroelectricity is by measuring the displacement (*D-E*) loop, which requires fabrication of a parallel plate capacitor from the material under test. The capacitor is put in a series configuration with a reference capacitor. Typically an alternating bias of triangular form with a certain frequency is applied, and the voltage drop over the reference capacitor hence charge is measured. Since capacitors are in series the measured charge of the reference capacitor is then equivalent to the charges on the capacitor under test. A schematic polarization loop of a ferroelectric is shown in Figure 2e.

At low fields almost all ferroelectrics behave as linear dielectrics. The hysteretic loop only opens at high fields where nonlinear polarization is dominant. The low field displacement responses, known as inner loops are schematically shown in Figure 2e-f. Despite its simplicity, one should pay attention not to merely rely on the displacement loop measurements. To highlight two common misleading loops we schematically present displacement curves for both linear and non-linear dielectrics for the ideal and slightly conductive cases. For the case of an ideal dielectrics no hysteresis is observed, Figures 2a and 2c. Slightly conductive dielectrics show hysteresis in their *D-E* loop, which appears due to the accumulation of conduction charges on the reference capacitor, as shown in Figures 2b and 2d for linear and non-linear dielectrics, respectively. Such *D-E* loops can be mistakenly interpreted as ferroelectric polarization. The *D-E* loops for ideal and non-ideal ferroelectrics are shown schematically in Figures 2e and 2f. Note the similarity between Figures 2d and 2f, albeit originating from two different mechanisms. To distinguish ferroelectric loops form non-ferroelectric ones, complementary electrical measurements are required.

Parasitic effects can be ruled out by a complementary test called shunt resistance wherein the reference capacitor is replaced with a reference resistor to measure instead of charge, the displacement current, $i = dQ/dt$, where Q is the charge passing through the circuit in unit time. Ferroelectrics, as schematically shown in Figure 2g-h, show two distinct peaks in their current response due to polarization switching. One can therefore easily distinguish between hysteresis caused by conduction and the ferroelectric one because hysteresis due to conduction does not contain any switching peak contributions.

We note one should also be careful about the shunt measurements as other parasitic effects can produce current peaks in the shunt measurements.[40] Such misleading current loops are typically characteristics of materials with low ionic conductivities.

As a good experimental practice, it is highly advisable to conduct electrical measurements in a dry atmosphere and preferably under vacuum. Since shunt measurement and *D-E* loop require the same equipment it is highly advisable to perform and report both loops. Since ferroelectrics behave linearly at small electric fields, measurement of polarization loops at biases well-below coercive voltages should result in the inner loops in Figure 1 e and f, undistinguishable of the *D-E* loops of linear dielectrics, as shown in Figure 2b.

To further verify ferroelectricity of the material under test, it is highly advisable to measure capacitance as a function of bias and derive the dielectric constant which for ferroelectrics shows a butterfly loop in response to the applied bias as schematically shown in Figure 2i.

To eliminate the effect of the parasitic currents due to leakage and conduction on polarization measurements, a pulsed technique called PUND can be used. In a PUND measurement, first a known polarization is set in the sample. Then a train of two pulses of the same polarity is applied, as shown schematically in Figure 2j. The response to the first pulse contains both switching and parasitic currents, whereas the second response contains only parasitic currents. Subtracting the two gives the net switching current whose integration with time give the net remnant polarization of the sample. The electrical measurement methods has been discussed in detail in recent reviews.[41,42]

We conclude this section with the statement that ferroelectricity of a new compound can be claimed when at least the set following measurements have been performed: XRD, dielectric spectroscopy to measure ε as function of temperature, polarization and switching current loops and the PUND.

3. Ferroelectric metal-organic frameworks

Since, the developments in the field of ferroelectric MOFs until 2012 have already been extensively reviewed,[43-45] we focus on the ferroelectric MOF literature published since 2012. Papers were retrieved using Web of Science and Google Scholar with the search term “ferroelectric metal organic framework”. A summary of the reported MOFs, the structural-physical characterization and the proposed ferroelectricity mechanism is given in Table 1. Here we first discuss the structural and then electrical characterizations. Subsequently we discuss the mechanism proposed for ferroelectricity.

3.1. Structural characterization

Three major routes have been explored to induce non-centrosymmetry in metal-organic frameworks. MOFs constructed with building blocks with 3-fold rotational symmetry[46,47] or a chiral center[48] have been extensively studied for their non-linear optical properties due to their non-centrosymmetric structures. Another route has been adding non-coordinating polar groups to the linker molecule to create non-centrosymmtric crystal structures.[49,50]

With regard to MOF papers reporting ferroelectricity they generally provide crystallographic analyses and report the crystal structure and its symmetry. Almost, all the reported compounds lack inversion symmetry as the prerequisite for ferroelectricity, except one compound[69] with centrosymmetric hexagonal structure, for which the observed D-E hysteresis behaviour is attributed to guest water molecules. We note that a significant amount of the reported MOFs contain water in their structure. It has been argued, particularly for chiral MOFs that presence of water molecules can induce the crystal to go to a non-centrosymmetric configuration.[69]

SHG has been employed to probe polarity of several MOF crystals highlighted in Table 1. Usually a near-infrared laser is used and the visible response of the MOF has been detected. Typically the presence of an SHG response has been reported to confirm the non-centrosymmetric structure. and no further analysis is carried out. SHG is a powerful optical spectroscopy technique, thorough and dedicated SHG studies on ferroelectric MOFs are still scarce.

Even though that for most MOFs the determination of the nonlinear optical efficiency was done in a semi-quantitative manner with the Kurtz powder method,[51] it seems that the response can be quite impressive for several non-centrosymmetrical MOFs.[52,53]

Numerous papers report pyroelectricity of MOFs,as highlighted in Table 1 by *dP/dT*, from which we extracted the Curie temperature for the compounds. Curie temperatures have also been reported using *ε-T* measurements. In some cases there is a substantial difference in T_c values for the same MOF compound. It must be noted however that being pyroelectric does not warrant *per se* ferroelectricity.

It is striking that despite the presence of well stablished electro-mechanical techniques MOFs have rarely been characterized for their piezoelectric properties. There is only one paper that discusses piezo properties of a chiral MOF compound that crystalizes in the C_2 point group with d_{22} value of ~7 pC/N.[54] Similarly there is only one report in which PFM is performed on MOF.[57] Details of the measurement and the method employed to exclude the non-ferroelectric contributions in the PFM signal however has not been discussed. We note that there is an immediate need to characterize MOFs for their electromechanical piezo response either using electromechanical techniques or with PFM.

Table 1. Overview of metal-organic frameworks related to ferroelectricity.

chemical formula	XRD (symmetry)	Complementary structural methods (confirmation polarity)	ε-T anomaly (Tc (K))	Swayer-Tower					Complementary electrical method	Proposed Mechanism
				E_c (KV/cm)[b]	P_s (μC/cm^2) [b],[c]	P_r (μC/cm^2) [b]	Frequency (Hz)	Contacting method / sample form		
[Co(titb)(L)]·3H_2O with H_2L=4,4′-(ethene-1,2-diyl)dibenzoic acid (H2L) and titb = 1,3,5-tris(imidazol-1-ylmethyl)-2,4,6-trimethylbenzene[55]										
	monoclinic (Cc)	-	-	9,12	0,063	0,044	-	-	-	-
[$NH_3(CH_2)_4NH_3$].[Mn_2 ($HCOO)_6$][56]										
	trigonal (P31c)	dP/dT	350	-	-	-	-	-	-	Water induced
[$H_2N(CH_3)2$][Ba(H_2O)(BTB)][57]										
	orthorohmbic ($Pna2_1$)	-	-	-	-	-	-	-	PFM	Ion motion in pores and channel
[$C_2H_5NH_3$][$Na_{0.5}Fe_{0.5}$ ($HCOO)_3$][58]										
	monoclinic (Pm)	SHG	365	-	-	0.2-0.8[d]	-	-	-	perovskite type, order-disorder amine cations
[Mn(4-tzba)$(bpy)_2$· 2O](bpy)·3H_2O With tzba=4-tetrazolbenzoic acid; bpy=2,2′-bipyridine)[59]										
	orthorohmbic ($Pna2_1$)	SHG	392	-	-	-	-	-	-	-
[$(CH_3)_2NH_2$]Fe($HCOO)_3$ [60]										
	trigonal (R3C)	dP/dT	164	1,25	~1	0,6	-	silver paste	-	-
[$CuL_2(H_2O)_2$]·($NO_3)_2$·($H_2O)_{1.5}$· (CH_3OH) with L = [$PhPO(NH_4Py)_2$][61]										
	monoclinic (Cs)	-	313	5.9 (9.7)	21.79 (18.35)	27.95 (28.53)	0,1	Al tape / discs	-	-
[Zn_2(mtz)$(nic)_2$(OH)]·0.5nH_2O with Hphtz = 5-phenyltetrazole, Hnic = nicotinic acid [62]										
	orthorhombic (C2v)	-	-	2,57	6,26	2,9	-		-	-
[Zn(phtz)(nic)]with Hphtz = 5-phenyltetrazole, Hnic = nicotinic acid [62]										
	monoclinic (Cs)	-	-	1,42	5,27	2,5	-	-	-	-

{[Fe(2,2′-bipyridine)$(CN)_4]_2$ Co-(4,4′-bipyridine)}·$4H_2O$[63]										
	monoclinic (C2 or Cm)	dP/dT	220	15 (10 K)	0.5 (10 K)	0.5 (10 K)	-	-	PUND	charge-transferred Fe^{2+}–Co^{3+}–Fe^{3+}
$[Cu_4O(Lvcz)_2Br_4]$·H_2O HLvcz=voriconazole [64]										
	triclinic (P1)	SHG		0,128	0,093	0,0455	-	-	-	-
$[Cu_2(HLvcz)_2I_2]$·H_2O HLvcz = voriconazole[64]										
	triclinic (P1)	SHG	350	0,0838	0,098	0,0589	-	-	-	-
$[[Ag(HLvcz)_2]CF_3SO_3$ Lvcz=voriconazole[64]										
	triclinic (P1)	SHG		0,0657	0,112	0,0571	-	-	-	-
$[Zn(s\text{-}nip)_2]$ s-nip=(*S*)-2-(1,8-naphthalimido)-3-(4-imidazole)propanoate[65]										
	monoclinic ($P2_1$)	-	~ 300	4,08	0,294	0,035	-	-	-	-
$[Co(s\text{-}nip)_2]\cdot(H_2O)_{0.5}$ with s-nip = (S)-2-(1,8-naphthalimido)-3-(4-imidazole)propanoate [65]										
	monoclinic ($P2_1$)	-	~ 300	3,68	0,0332	0,013	-	-	-	-
$[Cd_3(S\text{-}L)_4]\cdot(ClO_4)_2$ with L = 2-(1-(2-pyridine)-ethylimino)-5-bromo-6-methoxy-pheno [66]										
	monoclinic ($P2_1$)	-		1,47	0.08	0,035	-	silver paste	-	-
$[Cd(L_2)_2]_3.4H_2O$ with H_2L= 2- aminoisonicotinic acid[67]										
	trigonal (C3v)	-	~ 373	8,45	0.024	0,007	-	-	-	-
[Cd(tib)(p-BDC-OH)] . H_2O with tib = 1,3,5-tris(1-imidazolyl)benzene, p-H2BDC-R = 2-R-1,4-benzenedicarboxylic acid [68]										
	monoclinic ($P4_1$)	-	-	~1.2	11.65	6,65	-	-	-	-
$[InC_{16}H_{11}N_2O_8]\cdot1.5H_2O$[69]										
	hexagonal (P6222)[e]	-	144-158[a]	1,65	3.81	1,64	0.2 Hz-200kHz	Ag /MOF/ tungsten	-	water induced
$[(CH_3)_2NH_2]Fe(HCOO)_3$[70]										
		SHG, dP/dT	164			-		-	-	perovskite type, order-disorder amine cation
$[Cu_2L_4(H_2O)2]\cdot(ClO_4)_4\cdot(H_2O)_5\cdot(CH_3OH)$ with L=PhPO(NH-3-pyridyl)$_2$[71]										
	trigonal (R3)	-	-	16	1,8	-	0,1	powder	-	-
$[Cu_3L_6(H_2O)_3]\cdot(ClO_4)_5\cdot(NO_3)\cdot(H_2O)_{11}$ with L=PhPO(NH-3-pyridyl)$_2$[71]										
	trigonal	-	-	30	0,55	-	0,1	powder	-	-

	(R3)									
$[Fe(tib)_{2/3}(H_2O)_4[SO_4]$ with tib=1,3,5-tris(1-imidazolyl) benzene[72]										
	trigonal (R3)	-	~ 293	0,4	0,029	0,27	400-2000	powder	-	-
$[Ce_2(H_2O)_3(D\text{-}tar)_3]\cdot 3H_2O$ with tar=tartrate[73]										
	triclinic (P1)	-		0,579	0,233	0,009	-	powder	-	-
$[Ce_2(H_2O)_3(L\text{-}tar)_3]\cdot 3H_2O$ with tar=tartrate[73]										
	triclinic (P1)	-	-	0,505	0,171	0,015	-	powder	-	-
$Cu_2(bpy)(H_2O)(Clma)_2$ with Hclma = R-2-chloromandelic acid and bpe = 4,4'-dipyridine[74]										
	monoclinic ($P2_1$)	-	-	21,4	0,167	0,008	-	powder	-	-
Cu(bpp)(Clma) with Hclma = R-2-chloromandelic acid and bpp = 1,3-di(4-pyridyl)propane[74]										
	monoclinic ($P2_1$)	-	-	1,69	0,183	0,021	-	powder	-	-
$[(CH_3)_2NH_2][Mn\ (HCOO)_3]$[75]										
	monoclinic (Cc)	Brillouin scattering	-	-	-	-	-	-	-	perovskite type, order-disorder amine cations
$[Ag_2(HPIDC)]$ with H_3PIDC = (pyridin-4-yl)-1H-imidazole-4,5-dicarboxylaic acid[76]										
	monoclinic (Cc)	SHG	-	2,65	0,48	0,27	-	powder	-	-
$Zn_3(titmb)(BTC)_2(H_2O)$ with titmb = 1,3,5-tris(1-imidazol-1-ylmethyl)-2,4,6-trimethylbenzene and H_3BTC = 1,3,5-benzene-tricarboxylic acid[77]										
	monoclinic ($P2_1$)	SHG	-	0,68	0,0486	0,0144	-	powder	-	-
$[Mn(H_2O)_2(bpe)(SO_4)]\cdot H_2O$ with bpe=trans-1,2-bis(4-pyridyl)ethene[78]										
	monoclinic (C_2)	-	-	8,8	0,4177	0,28895	-	powder	-	-
$\{Co_2(L)\text{-}(bpe)(H_2O)\}.5H_2O$ with H_4L = N-(1,3-dicarboxy-5-benzyl)-carboxymethylglycine[79]										
	hexagonal ($P6_1$)	-	320	1	2,6	1	-	single crystal	-	water guest molecules
[Zn(Mitz)Cl] with Mitz = 3-tetrazolyl-6-methyl-5-(4-pyridyl)-2-pyridone[80]										
	orthorombic ($Pna2_1$)	SHG	-	2,6	0,51	0,21	-	powder	-	-
$[Mn(tib)_2(H_2O)_4]SO_4$ with tib = 1,3,5-tris(1-imidazolyl) benzene[80]										
	rhombohedral (R3c)	-	278	2	0,208	0,586	-	powder	-	-
$[Co(tib)_2(H_2O)_4]SO_4$ with tib = 1,3,5-tris(1-imidazolyl) benzene[80]										

	rhombohedral (R3c)	-	290	2,6	0,383	0,208	-	powder	-	-
[Sr(μ-BDC)(DMF)] with BDC = benzene-1,4-dicarboxylate[81]										
	trigonal ($P3_1$)	-	-	7,1	0,025	0,018	16,7	powder	-	Induced by DMF molecules
[Sr(μ-BDC)(DMF)] with BDC = benzene-1,4-dicarboxylate[82]										
	trigonal ($P3_1$)	-	-	0,81	0,83	0,48	-	single crystal	-	guest DMF molecules
Co(SDBA)(BIMB) with H_2SDBA = 4,4′-dicarboxybiphenylsulfone and bimb = 4,4′-bis(1-imidazolyl)biphenyl[83]										
	monoclinic (Cc)	-	-	3,38	0,238	0,051	-	powder	-	-
$Mg(int)_2 \cdot H_2O$ with int = isonicotinate[84]										
	monoclinic ($P2_1$)	-	-	~ 2	~0,016	~0,0075	-	single crystal	-	-
$[Sm(HCOO)_3]$[85]										
	trigonal (R3m)	-	-	6,59	0,4	0,026	-	powder	-	-
$[Cd(BDAC)]_2.H_2O$ with HBDAC = (1'H-[2, 2']biimidazoly-1-yl)-acetic acid[86]										
	orthorhombic (Ccc2)	-	-	1,493	1,14	0,91	-	-	-	-
$[Zn_2(TPOM)(5\text{-OH-bdc})_2] \cdot (DMF)(H_2O)_2$ with TPOM = tetrakis(4-pyridyloxymethylene)methane[87]										
	monoclinic (P2)	-	-	5,755	0,451	0,052	-	crystal sample plate	-	-
$[Cd(pmida)H_2O] \cdot 1.8\ H_2O]$ with pmida = N-(4-pyridylmethyl)iminodiacetate[88]										
	Orthorombic ($Pna2_1$)	SHG	-	37,5	~1,75	0,605	-	single crystal	-	-
$[Cd_3(BPT)_2(H_2O)_9] \cdot 2H_2O$ with BPT = biphenyl-3,4′,5-tricarboxylate[89]										
	monoclinic (C2)	SHG	-	10,48	0,039	0,025	-	powder	-	-
$[Ni_2(bptc)(en)_2(m2\text{-}H_2O)].2H_2O$ with H_4bptc = biphenyl-2,5,20,50-tetracarboxylic acid, en = ethylenediamine[90]										
	orthorhomic (Fdd2)	-	-	Not reported	-	-	-	single crystal	-	-
$[Cd_6(L)_4(Cam)_4(H_2O)_4] \cdot 2H_2O$ with H_2Cam = enantiopure camphoric acid[91]										
	monoclinic (C2)	SHG	-	17,11		0,14	-	-	-	-
$[Co(BIPA)(titmb)] \cdot H_2O$ with H_2BIPA = 5-bromoisophthalic acid and titmb = 1,3,5-tris(imidazol-1-ylmethyl)-2,4,6-tri-methylbenzene[92]										
	orthorombic ($Pna2_1$)	SHG	-	0,5	0,06	0,016	-	powder	-	-
$[CX_3CH_2YH_3]Mn(HCOO)_3$ with X=H or F, Y=N or P[93]										

	orthorombic ($Pna2_1$)	-	-	-	-	2-6[d]	-	-	-	perovskite type, order-disorder amine cations
$[C(NH_2)_3]Cu[(HCOO)_3]$[94]										
	orthorombic ($Pna2_1$)			-	-	0,37[d]	-	-	-	perovskite type, order-disorder amine cations
$[C(NH_2)_3]Cu[(HCOO)_3]$[125]										
	orthorombic ($Pna2_1$)	dP/dT	265	-	-	0,11[f]	-	-	-	perovskite type, order-disorder amine cations
$[(CH_3)_2NH_2]M[(HCOO)_3]$ with M = Co or Mn[95]										
	Trigonal (R3c)	RUS	165 (Co), 185 (Mn)	-	-	-	-	-	-	perovskite type, order-disorder amine cations
$[(CH_3)_2NH_2]Mg[(HCOO)_3]$[122]										
	monoclinic (Cc)	-	270	-	-	-	-	-	-	perovskite type, order-disorder amine cations
$[(CH_3)_2NH_2]Co[(HCOO)_3]$[96]										
	monoclinic (Cc)	dP/dT	140-230[a]	5 (100K) 2,5 (150 K)	1 (100 and 150K)	0,6 (100K) 0,25 (150 K)	-	powder	-	perovskite type, order-disorder amine cations
$[(CD_3)_2(ND_2)_3]Co[(DCOO)_3]$[97]										
	monoclinic (Cc)	SHG	151	7 (136K)	1 (136K)	0,7 (136K)	-	-	-	perovskite type, order-disorder amine cations
$[NH_4][Zn(HCOO)_3]$[98]										
	hexagonal ($P6_3$)	-	181	2,8 (163K)	1,03 (163K)	0,68 (163K)	-	single crystal	-	perovskite type, order-disorder amine cations
$[NH_4][Mg(HCOO)_3]$[123]										
	hexagonal ($P6_3$)	-								perovskite type, order-disorder amine cations
$Mn_5(NH_2bdc)_5(bimb)_5$.[99]										
	monoclinic (Cc)	-	-	0,35	2,556	1,2	-	single crystal	-	-

[a] frequency dependent
[b] Measurements were carried out at temperature if not mentioned otherwise.
[c] P_s was taken at the maximum applied field (typically below 10 kV/m).
[d] Calculated polarization.
[e] Reported crystal structure is centrosymmetric.
[f] The polarization was calculated from the pyroelectric current after poling at E=±6kV from 300 to 150 K.

Electrical characterizations: First we note that measurement of *D-E* loop at different biases (well-below coercive voltages) to obtain the inner loops and at different frequencies, as shown in Figure 2g, are mostly missing from the literature.

Typically, coercive fields less than 5 kV/cm have been reported for ferroelectric MOFs. Some of the values reported E_c does not make any physical sense such as those with E_c well below 1 kV/cm, which translate to voltages of 0.1 V for a layer of 1 µm thick. Such values are extremely low compared to conventional ferroelectrics such as BTO (10 kV/cm),[100] PZT (20 to 80 kV/cm)[101] and PVDF (500 kV/cm).[102] We note that E_c values as low as 5 kV/cm have only been reported for the state-of-art molecular ferroelectrics whose polarization loop was recorded at 422 K.[103] However substantially higher E_c at room temperature is expected even for molecular ferroelectrics since E_c is thermally activated. The majority of the *D-E* loops have been recorded at relatively low fields. Whether such low fields can polarize the material remains still an open question.

Reported remanent polarization values for the "ferroelectric" MOFs are typically well below 1 µC/cm^2. Values as low as 7 nC/cm^2 have also been reported. Measuring such low values in combination with the low E_c is an indicative of a slightly conductive dielectric rather than a ferroelectric, as shown in Figure 2b and 2d. In fact loops recorded at room temperature mostly look like to Fig. 2b even though that for some of the compounds an anomaly is reported in the dielectric constant as a function of temperature. It is surprising that usually the frequency at which the loops are recorded is recorded is not reported and that the *D-E* loops are not measured at different frequencies.

Generally a film consisting of MOF powder is used as capacitor in these measurements. However, it is not always mentioned in the literature how the parallel plate capacitor has been fabricated, how the MOF-film and contacts were made. A handful of reports mention silver paste or metal adhesive tapes as contact material, which in such case extra care should be taken. Silver past contain organic solvents and metal tapes contain an adhesive layer both of which can complicate data interpretation.

Using MOF single crystals, as compared to powder can be advantageous since the crystal can be directly contacted with metallic needles provided that the crystal is of decent size.

3.2. Mechanism of ferroelectricity in metal-organic frameworks

For a limited part of the reported MOFs a more thorough study of the ferroelectric properties has been provided. For these MOFs we provide a tentative overview of their mechanisms leading to ferroelectricity.

Polar guest induced ferroelectricity

This category discusses ferroelectricy induced by guest water or other polar molecules such as ethanol in metal-organic frameworks.[129,130] It has been shown for instance that $[InC_{16}H_{11}N_2O_8]\cdot 1.5H_2O$ is centrosymmetric in its dry form (hexagonal crystal structure with $P6_{222}$ point group symmetry). Exposure to moisture however induces a polar phase in the framework to which they attribute the source of the ferroelectric *D-E* hysteresis loop.[69]

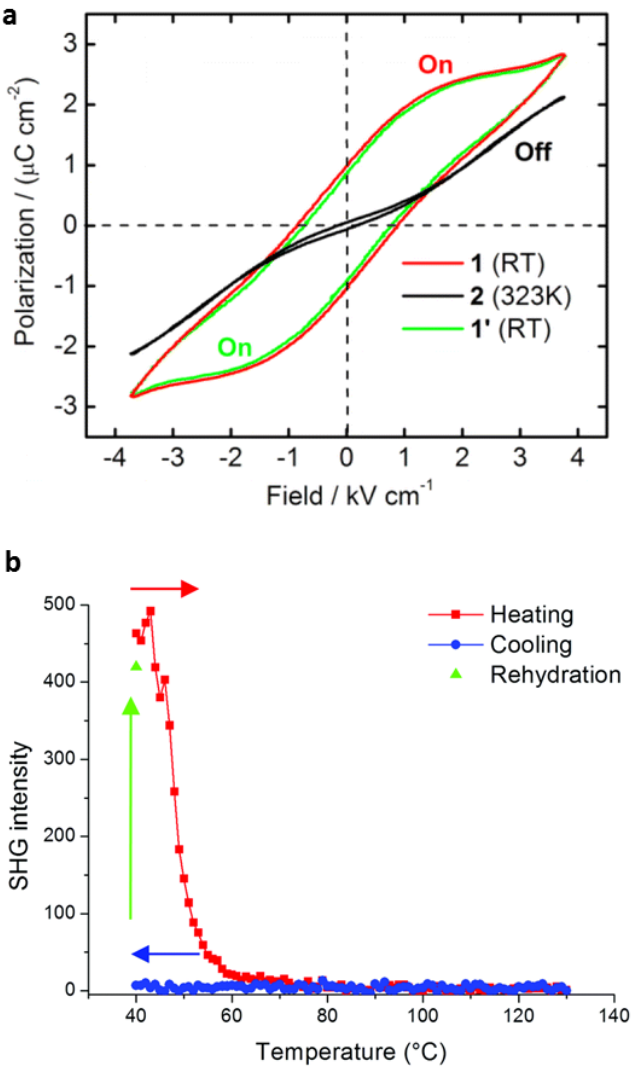

Figure 4. a) D-E loop of as synthesized, dehydrated and rehydrated compound $[\{Co_2(L)(bpe)(H_2O)\}\cdot 5H_2O]_n$. "Reprinted with permission from Journal of the American Chemical Society 2013, 135, 10214–10217. Copyright 2013 American Chemical Society."[79] b) SHG signal of Fe(OH/F)(BDC)·[butanol] during a heating/cooling/rehydration cycle. The SHG signal vanishes completely during heating under N_2 flow and remains zero upon cooling. Heating and cooling occurred at 1 K/min under N_2 flow. In a last step, the SHG activity was recovered by allowing H_2O molecules to enter the pores. Figure 3b is reproduced from Dalton Trans. 2016, 45, 4401-4406 - Published by The Royal Society of Chemistry.[50]

Dong *et al.*[79] have synthesized a helical MOF compound, $[\{Co_2(L)(bpe)(H_2O)\}\cdot 5H_2O]_n$, using cobalt(II) as the metal cluster and N-(1,3-dicarboxy-5-benzyl)-carboxymethylglycine (H_4L) as ligand. The MOF can accommodate ordered helical water streams in its helical grooves. Measured the *D-E* loop of the hydrated, dehydrated and rehydrated is given in Figure 4a. While the dehydrated MOF behaves as a non-linear dielectric, the hydrated form shows hysteretic response. A broad peak near 320 K was measured for the dielectric *ε-T* response of the MOF, which was ascribed to changes in the polarizability of H_2O molecules confined in the helical groove due to disorder or gasification.

Using SHG spectroscopy Markey et al.[50] have shown that while the fluor doped MIL-53(Fe) has a non-centrosymmetric lattice when the pores are filled with butanol. Upon heating under N_2 environment the butanol is removed, and the crystal transforms to a centrosymmetric one. Upon cooling in a water-free environment centrosymmetric crystal structure of the MOF is preserved since SHG activity was absent, as shown in Figure 4b. Upon rehydration, the SHG signal is back and the crystal transforms to its polar form. Interestingly the MOF also has a polar structure when the pores are filled with para-xylene, a centrosymmetric guest molecule.

Perovskite type ferroelectricity

A series of MOFs show the equivalent of a perovskite structure and follow the ABX_3 pattern in which A is typically a quaternary amine cation in the pores, B is a divalent metal ion (M^{2+}) and X is (formate)$^-$. The formate$^-$ and M^{2+} transition metal ions form as semicuboid anionic ReO_3–type structure an example of which is shown in Figure 5. The paraelectric-ferroelectric phase transition is ascribed to the disorder-order transition of the A cations trapped in the pores. In contrast to helical MOFs, in the perovskite like MOFs, the amine cations are locked in the cages and long range diffusion is not possible. Perovskite like MOFs are the most thoroughly studied class of ferroelectric MOFs. The M^{2+} transition metal ions can be chosen as such to induce ferromagnetic properties, making several of these perovskite MOFs multiferroic materials. As can be seen from Table 1, the perovskite MOF show polarization of typically around 1 μC/cm^2, and undergo the paraelectric-ferroelectric phase transition in a temperature range from 150 K to 200 K.

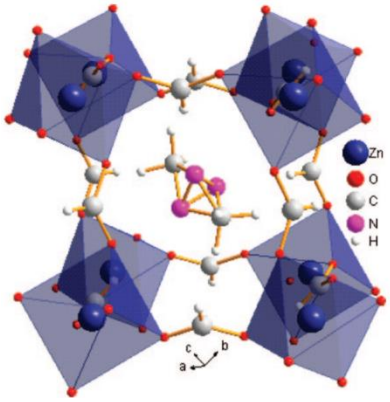

Figure 5. The crystal structure of $[(CH_3)_2NH_2]Zn(HCOO)_3$ that follows the perovskite ABX_3 structure with A = the quaternary amine in the cages, B = Zn^{2+} and X = formate linking the Zn octahedrons. "Reprinted with permission from Journal of the American Chemical Society 2008, 130, 10450-10451. Copyright 2008 American Chemical Society." [104]

The structures $[(CH_3)_2NH_2]M(HCOO)_3$ with M = Zn, Mn, Fe, Co or Ni were originally reported as antiferroelectric with a Curie temperature between 160-185K.[104,105] XRD of the compounds showed that the amine cation occupies one of the three equivalent positions with regard to the M–formate framework. Below the transition temperature the amine cation can only occupy two positions and become ordered. The order-disorder type ferroelectric-paraelectric transition has been confirmed for $[(CH_3)_2NH_2]Mn(HCOO)_3$, vibrations of the cation was probed by Raman spectroscopy, above the transition temperature the cation vibration appears as a single broad band due to the freedom of the cation to move between three equivalent positions, while below the transition temperature the vibrations split in multiple sharp lines.[106] The order-disorder transition was further confirmed by entropy changes upon phase transition of the crystal structures[75,97] and the ordering can be described by a three state 3-D Potts model.[107] We further note that order-disorder transitions have been confirmed using deuterated analogues of the MOF compound.[97,128] With Cr^{3+} doping of the material the phase transition temperature lowers, and its first order nature changes to partially diffused.[126]

$NH_4]Zn[HCOO]_3$ is the first perovskite-type MOF for which a ferroelectric *D-E* hysteresis loop has been reported. It has a Curie temperature of 191 K. The measured remnant polarization of 1.03 μC/cm^2 agrees well with the theoretically predicted value of 0.96 μC/cm^2 estimated from the ordered position of the NH_4^+ cations.[89] Ferroelectricity of $[(CH_3)_2NH_2]M(HCOO)_3]$ structures, more specifically the Co^{2+} MOF, was confirmed by measuring *D-E* hysteresis loop, and observation of second-harmonic generation response below the Curie temperature. The order-disorder transition was further unraveled for $[(CH_3)_2NH_2]Zn(HCOO)_3]$ with specific heat measurements and ^{1}H NMR measurements,[108] as well as with electron paramagnetic resonance (EPR) measurements when doped with Mn^{2+}.[109] Resonant ultrasound spectroscopy (RUS) and Brillouin scattering has been employed to study the paraelectric-ferroelectric phase transition further which both reconfirm the order-disorder phase transition mechanism.[95,110] Interestingly, the $[(CH_3)_2NH_2]M(HCOO)_3]$ compound with M = Mg^{2+} a much high transition temperature between a polar and centrosymmetric phase has been reported, namely 270K, albeit without a *D-E* hysteresis loop.[122] This was attributed to the more ioned Mg-O bonds leading to stronger H-bonds between the amine cation and the formate O atoms. Similarly the $[NH_4]Mg[HCOO]_3$ was synthesized to attempt to realize a higher Curie temperature than the Manganese containing compound, $[NH_4]Mn[HCOO]_3$ which has a T_c of 254 K.[123] The T_c of the Mg compound however was similar: 255 K.[124]

Density Functional Theory calculations have predicted that cations with more polarizable electron density can lead to higher remnant polarization.[94] It has been shown that by replacing the amine with a cation containing more electron negative elements, namely $CF_3CH_2PH_2$, the polarization can be increased from 2 μC/cm^2 to 6 μC/cm^2,[93] which is close to values typically reported for ferroelectric polymers.[111] We note however that despite the low remnant polarization, perovskite like MOFs are also heavily studied for their magnetic and multiferroic properties.[112,113,120,121]

Room temperature ferroelectricity in perovskite like MOFs is still an ongoing quest as it requires Curie temperatures that are polar well above 300 K. The perovskite MOF based on guanadimium $[(NH_2)_3C]Cu(HCOO)_3]$ shows a comparitively high Tc of 263 K. The modest polarization of 0,11 μC/cm^2 is caused by an induced dipole moment on the apolar cations $[(NH_2)_3C]^+$[125]. Recently a heterometallic perovskite MOF $[C_2H_5NH_3][Na_{0.5}Fe_{0.5}(HCOO)_3]$ has been reported that can show a dielectric anomaly has been observed around 360 K, which interestingly fulfils the Curie-Weiss law.[Fout! Bladwijzer niet gedefinieerd.] Observation of the order-disorder phase transition for the

compound can be suggestive of cation ordering at room temperature, which make this particular compound a potential candidate for the first room-temperature ferroelectric perovskite MOF. Polarization measurements have not been yet reported for this compound. In contrast another heterometallic perovskite MOF $[(C_2H_5)_2NH_2][Fe^{II}Fe^{III}(HCOO)_6]$ has also shown a dielectric anomaly, albeit at the much lower temperature of 240K. Whether the low temperature phase is non-centrosymmetric has not yet been reported.[126]

Charge transfer

Unique among metal-organic frameworks, the {[Fe(2,2′-bipyridine)$(CN)_4]_2$Co-(4,4′-bipyridine)}·$4H_2O$ framework (see Figure 6) shows ferroelectricity most likely through a mechanism of charge transfer upon cooling down. Below 220 K, the Fe^{3+} – Co^{2+}– Fe^{3+} motifs transit to Fe^{3+} – Co^{3+}– Fe^{2+} and thereby creating net dipole hence becomes a polar motifs. Application of an electric field can then switch Fe^{3+} – Co^{3+}– Fe^{2+} motifs into Fe^{2+} – Co^{3+}– Fe^{3+} motifs, hence switching the dipole direction and the polarity. Polarity of the low temperature phase has been confirmed with pyroelectric current measurements. The Curie temperature of 220 K has been reported and a polarization hysteresis loop obtained was obtained using PUND method at 10 K.[63] We note that water effects can be excluded as the loop was measured at cryogenic temperatures and polarization due to motion of water molecules can be ruled out.

The charge transfer mechanism in a metal-organic framework has been obtained by using a framework that is heterometallic wherein the metal centres are very closely positioned. Obtaining such frameworks from rational design is not a trivial task.

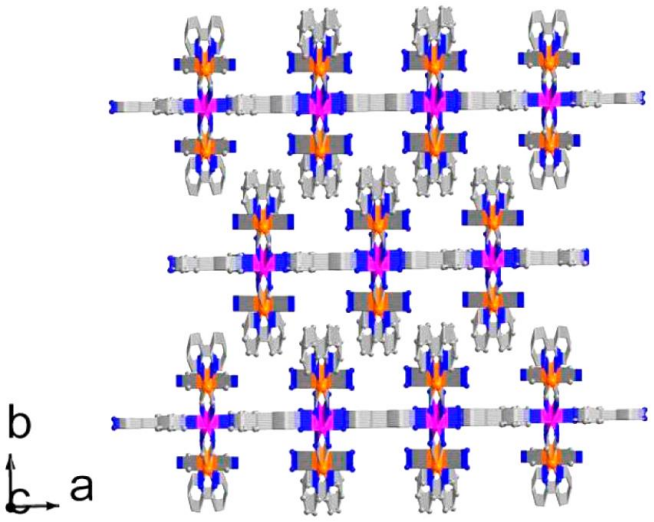

Figure 6. Packing diagram of the two-dimensional layers of Fe_2Co MOF. H atoms are omitted for clarity. Atomic scheme: Fe, orange; Co, purple; C, gray; N, blue. Reprinted with permission from Inorganic Chemistry 2015, 54, 6433–6438. Copyright 2015 American Chemical Society."[63]

3.3. Protocol for the identification of ferroelectricity in metal-organic frameworks

From the summary given in Table 1, it becomes clear that a general protocol for measuring ferroelectric properties in MOF is still missing. Therefore, here we outline the most relevant measurements to survey ferroelectric properties and suggest a protocol to report experimental data for new MOF compounds:

1- Determination of the *dry*-crystalline structure.
Hence, without guest molecules such as water, solvent, inside the pores. When the dry crystal falls into one of the categories listed in Table S1 (supporting info), then the framework itself can be potentially a ferroelectric. Complementary measurement such as presence of second harmonic generation response or observation of pyroelectric currents, can confirm the non-centrosymmetry and polarity of the crystal.

2. Fabrication of a parallel-plate capacitor.
To identify whether a polar structure is ferroelectric electrical measurements are needed, for which a parallel-plate capacitor is needed. As a good practice, device fabrication process should be reported with particular attention to the following points:
   a. How the MOF film was made? (*i.e.* single crystal, powder, thin-film, pressed powder disks, etc)
   b. What is the thickness of the MOF layer?
   c. What are the contacts and how are they defined? Contacts containing adhesive should be preferably avoided due to the unknown properties of the adhesive. Care should be taken using silver paste as it contains different organic solvents.
   d. What is the device area?
   e. What is the environment in which the measurement has taken place? (*e.g.* vacuum, ambient, temperature and humidity)
   f. Measurement of the dielectric constant of the (dehydrated) MOF as a function of temperature, to obtain the Curie temperature.
   g. Next to electric field, the voltages that are applied for polarization measurements should be reported.
   h. Measurements of the shunt loop to rule out hysteresis due to dielectric conductivity, which can be simply obtained by replacing the reference capacitor used for *D-E* loop with a known resistor.
   i. Report of the inner loops.
   j. PUND or Capacitance-voltage measurement can complement the loop measurements.
   k. Measurement of the *D-E* or shunt loops at different temperature. Switching peaks (or polarization) should disappear above Curie temperature.

A careful consideration of the abovementioned points would help to advance the field of ferroelectric MOF through reliable characterization of ferroelectricity in MOFs.

3.4. Outlook and challenges

The field of ferroelectric MOFs is still in its embryonic research phase. There are ambiguities as discussed above, that need clarifications, and still many fundamental open questions. Despite the wide application range of ferroelectrics. Synthesis of new ferroelectric MOFs and fundamental understanding as how to induce polarization in the crystal are of high priority. Here we

highlight some of the challenges that are lying ahead or can be tackled.

Room temperature ferroelectricity: There are at the moment only limited number of guest-free MOFs with a thorough characterization of their ferroelectric properties. These all show ferroelectricity at temperatures well below room temperature. For any application polarization switching at room temperature or above is desired. The quest is still ongoing as room temperature polarization loops with coercive field and polarisation values to clearly underpin their ferroelectricity have not been reported yet.

Thin-film capacitor: Fabrication of thin-film MOF has been a long standing challenge.[114]A review of the used techniques is provided in reference 115.[115] Recently MOF thin-films have been synthesized epitaxially on a substrate by chemical vapour deposition.[116] Conventional photolithography was carried and complex structures of the MOF thin-film were realized. It is evident that for fundamental studies a reproducible platform is required. Thin-film capacitors are the primary device to fabricate and realization of the ferroelectric MOF thin-films is crucial to that end.

Piezoelectric characterization: So far the electro-mechanical properties of (ferroelectric) MOFs have hardly been tackled. As ferroelectrics are all piezoelectrics, knowledge on the piezo properties of MOF would provide a better understanding of the ferroelectric properties. Studies of the strain-stress under an applied field are of paramount importance. Porous ferroelectrics, wherein porosity is introduced in a disordered manner via processing tricks, are becoming a new trend for energy harvesting applications[117] MOFs are inherently well-ordered porous structures that can perhaps show unconventional electro-mechanical properties.

Multi-functional MOFs: There is great degree of freedom in the choice of metallic clusters and the linkers for the synthesis of a MOF compound. One can therefore integrate different, even mutually exclusive properties in a single compound of which multi-ferroic MOFs are a good example.[118,119] Other orthogonal properties such as luminescent ferroelectrics can be scientifically interesting.

4. Conclusions

We briefly discussed ferroelectricity and primary methods to survey ferroelectric properties in a new compound. We highlighted the latest development in the field of ferroelectric MOFs. Three mechanisms leading to ferroelectricity have been identified and critically discussed. Based on the shortcoming present in the literature, we have presented a protocol for the study of ferroelectricity in MOF compounds. We have presented an outlook and highlighted the missing pieces of the puzzle “ferroelectric MOFs”.

Acknowledgements. K.A. acknowledges Alexander von Humboldt Foundation for the funding provided in the framework of the Sofja Kovalevskaja Award endowed by the Federal Ministry of Education and Research, Germany. M.v.d.V. acknowledges the Ducth Science Foundation (NWO) and the Dutch Polymer Institute for a NEWPOL grant (project number 731.015.506). The authors wish to thank D. M. de Leeuw and K. Markey for fruitful discussions.

Keywords: metal-organic frameworks • coordination polymers • ferroelectricity

[1] G. Ferey, *Chem. Soc. Rev.* **2008**, *37*, 191-214.
[2] L. E. Kreno, K. Leong, O. K. Farha, M. Allendorf, R. P. Van Duyne, J. T. Hupp *Chem. Rev.* **2012**, *112* , 1105–1125.
[3] H. Furukawa, K. E. Cordova, M. O’Keeffe, O. M. Yaghi, *Science* **2013**, *341*, 1230444.
[4] M. D. Allendorf, C. A. Bauer, R. K. Bhakta, R. J. T. Houk, *Chem. Soc. Rev.* **2009**, *38*, 1330-1352.
[5] Y. Cui, Y. Yue, G. Qian, B. Chen, *Chem. Rev.* **2012**, *112*, 1126–1162.
[6] M. Kurmoo, *Chem. Soc. Rev.* **2009**, *38*, 1353-1379.
[7] C. G. Silva , A. Corma, H. Garcia *J. Mater. Chem.* **2010**, *20*, 3141-3156.
[8] M. Alvaro, E. Carbonell, B. Ferrer, F. X. L. Xamena, H. Garcia *Chem. Eur. J.* **2007**, *12*, 5106-5112.
[9] H. Xu, R. Chen, Q. Sun, W. Lai, Q. Su, W. Huang, X. Liu *Chem. Soc. Rev.* **2014**, *43*, 3259-3302.
[10] J. Valasek, *Phys. Rev.* **1921**, *17*, 475–481.
[11] A. von Hippel, R. G. Breckenridge, F. G. Chesley and L. Tisza, *Ind. Eng. Chem.* **1946**, *38*, 1097-1109.
[12] H. Kawai, *Jpn. J. Appl. Phys.*, **1969**, *8*, 975-976.
[13] J. G. Bergman, J. H. McFee and G. R. Crane, *Appl. Phys. Lett.*, **1971**, *18*, 203-205.
[14] R. G. Kepler and R. A. Anderson, *J. Appl. Phys.*, **1978**, *49*, 1232-1235.
[15] S. Horiuchi, Y. Tokunaga, G. Giovannetti, S. Picozzi, H. Itoh, R. Shimano, R. Kumai, Y. Tokura *Nature* **2010** , *463*, 789-792.
[16] P.-P. Shi, Y.-Y. Tang, P.-F. Li, W.-Q. Liao, Z.-X. Wang, Q. Ye, R.-G. Xiong *Chem. Soc. Rev*. **2016**, 45, 3811-3827.
[17] W.-Q. Liao, Y. Zhang, C.-L. Hu, J.-G. Mao, H.-Y. Ye, P.-F. Li, S. D. Huang, R.-G. Xiong *Nature Communications* **2015**, 6, 7338.
[18] H.-Y. Ye , W.-Q. Liao, C.-L. Hu , Y. Zhang , Y.-M. You, J.-G. Mao, P.-F. Li , R.-G. Xiong *Advanced Materials* **2016**, 28, 2579–2586.
[19] Z. Hu, M. Tian, B. Nysten, A.M. Jonas *Nature Mater*. **2009**, *8*, 62-67.
[20] M. Guo, H. L. Cai, R. G. Xiong *Inorg. Chem. Commun.* **2010**, *13*, 1590-1598.
[21] W. Zhang, R. G. Xiong *Chem. Rev.* **2012**, *112*, 1163-1195.
[22] J. Li, Y. Liu, Y. Zhang, H. L. Cai, R. G. Xiong, *Phys. Chem. Chem. Phys.* **2013**, *15*, 20786-20796.
[23] M. E. Lines and A. M. Glass, *Principles and Applications of Ferroelectrics and Related Materials*, Oxford University Press, **1977**.
[24] N. Setter, D. Damjanovic, L. Eng, G. Fox, S. Gevorgian, S. Hong, A. Kingon, H. Kohlstedt, N. Y. Park, G. B. Stephenson, I. Stolitchnov, A. K. Taganstev, D. V. Taylor, T. Yamada, S. Streiffer, *J. Appl. Phys.* **2006**, *100*, 051606.
[25] R .C. G. Naber, K. Asadi, P. W. M. Blom, D. M. de Leeuw, Bert de Boer *Adv. Mater.* **2010**, *22*, 933-945.
[26] J. F. Scott, *Science* **2007**, *315*, 954-959.
[27] M. Dawber, K. M. Rabe, J. F. Scott *Rev. Mod. Phys.* **2005**, *77*, 1083-1130.
[28] J. F. Nye, *Physical Properties of Crystals*, Clarendon Press, **1957**.
[29] J. F. Scott *J. Phys.: Condens. Matter* **2008**, *20,* 021001.
[30] S. B. Lang, *Physics Today* **2005**, *58*, 31-36.
[31] S. B. Lang, *Sourcebook of Pyroelectricity*, Gordon & Breach Science Publishers, Inc., 1974.
[32] S. A. Denev, T. T. A. Lummen, E. Barnes, A. Kumar, V. Gopalan *J. Am. Ceram. Soc.* **2011**, *94*, 2699-2727.
[33] a) M. A. van der Veen, F. Vermoortele, D. De Vos, T. Verbiest *Anal. Chem.* **2012**, *84*, 6378-6385; b) M. A. van der Veen, F. Vermoortele, D. De Vos, T. Verbiest *Anal. Chem.* **2012**, *84*, 6386-6390.
[34] Markys G. Cain (Editor), *Characterization of Ferroelectric Bulk Materials and Thin Films.* Springer **2014**.
[35] E. Defay (Editor), *Integration of Ferroelectric and Piezoelectric Thin Films: Concepts and Applications for Microsystems*, Wiley-ISTE **2011**.
[36] S. V. Kalinin, B. J. Rodriguez, S. Jesse, J. Shin, A. P. Baddorf, P.

Gupta, H. Jain, D. B. Williams, A. Gruverman, *Microsc. Microanal.* **2006**, *12*, 206-220.
[37] A. L. Kholkin , V. V. Shvartsman , D. A. Kiselev & I. K. Bdikin *Ferroelectrics* **2006**, 341, 3-19.
[38] A. Gruverman, O. Auciello, H. Tokumoto, *Annu. Rev. Mater. Sci.* **1998**, *28*,101-123.
[39] N. Balke, P. Maksymovych, S. Jesse, A. Herklotz, A. Tselev, C. B. Eom, I. I. Kravchenko, P. Yu, S. V. Kalinin *ACS Nano* **2015**, *9*, 6484–6492.
[40] J. Li, H. F. Zhang, G. Q. Shao, B. L. Wu, S. X. Ouyang *EPL*, **2014**, *108*, 27005.
[41] L. Jin, F. Li, S. Zhang, *J. Am. Ceram. Soc.* **2014**, *97*, 1-27.
[42] T. Schenk, E. Yurchuk, S. Mueller, U. Schroeder, S. Starschich, U. Böttger, T. Mikolajick *Appl. Phys. Rev.* **2014**, *1*, 041103.
[43] M. Guo, H. L. Cai, R. G. Xiong *Inorg. Chem. Commun.* **2010**, *13*, 1590-1598.
[44] W. Zhang, R. G. Xiong *Chem. Rev*. **2012**, *112*, 1163-1195.
[45] J. Li, Y. Liu, Y. Zhang, H. L. Cai, R. G. Xiong, *Phys. Chem. Chem. Phys.* **2013**, *15*, 20786-20796.
[46] a) O. R. Evans, R. G. Xiong, Z. Y. Wang, G. K. Wong, W. Lin, *Angew. Chem., Int. Ed.* **1999**, *38*, 536-538; b) O. R. Evans, Z. Wang, R. G . Xiong, B. M. Foxman, W. Lin, *Inorg. Chem.* **1999**, *38*, 2969-2973; c) W. Lin, L. Ma, O. R. Evans, *Chem. Commun.* **2000**, 2263-2264.
[47] a) W. Lin, Z. Y. Wang, L. Ma *J. Am. Chem. Soc.* **1999**, *121*, 11249-11250; b) Y. Liu, G. Li, X. Li, Y. Cui, *Angew. Chem., Int. Ed.* **2007**, *46*, 6301-6304. c) Y. Liu, X. Xu, F. K. Zheng, Y. Cui, *Angew. Chem., Int. Ed.* **2008**, *47*, 4538-4541.
[48] a) H. Zhao, Y. H. Li, X. S. Wang, Z. R. Qu, L. Z. Wang, R. G. Xiong, B. F. Abrahams, Z. Xue *Chem. Eur. J.* **2004**, *10*, 2386–2390; b) Q. Ye, Y. H. Li, Q. Wu, Y. M. Song, J. X. Wang, H. Zhao, R. G. Xiong, Z. Xue *Chem. Eur. J.* **2005**, *11*, 988–994; c) A. Ferguson, L. Stefanus J. Tapperwijn, F. X. Coudert, S. Van Cleuvenbergen, T. Verbiest, M. A. van der Veen, S. G. Telfer, *Nature Chem.* **2016**, *8*, 250-257.
[49] a) H. Reinsch, M. A. van der Veen, B. Gil, T. Verbiest, D. De Vos, N. Stock *Chem. Mater.* **2013**, *25*, 17-26; b) P. Serra-Crespo, M. A. van der Veen, E. Gobechiya, K. Houthoofd, Y. Filinchuk, C. Kirschhock, J. Martens, B. Sels, D. De Vos, F. Kapteijn, J. Gascon, *J. Am. Chem. Soc.* **2012**, *134*, 8314-8317.
[50] K. Markey, T. Putzeys, P. Horcajada, T. Devic, N. Guillou, M. Wubbenhorst, S. Vancleuvenbergen, T. Verbiest, D. De Vos, M.A. van der Veen, *Dalton Trans.* **2016**, *45*, 4401-4406.
[51] a) J. Zyss,D. S. Chemla in *Nonlinear Optical Properties of Organic Molecules and Crystals*, (Eds. D. S. Chemla, J. Zyss), Elsevier, **1987**, pp 23-191; b) R. T. Bailey, G. Bourhill, F. R. Cruickshank, D. Pugh, J. N. Sherwood, G. S. Simpson, *J. Appl. Phys.* **1993**, *73*, 1591-1597. c) M. A. van der Veen, T. Verbiest, D. E. De Vos, *Microporous Mesoporous Mater.* **2013**, *166*, 102-108.
[52] C. Wang, T. Zhang, W. Lin, *Chem. Rev.* **2012**, *112*, 1084-1104.
[53] a) T. Seidler, B. Champagne, *J. Phys. Chem. C*, **2016**, *120*, 6741-6749; b) S. Van Cleuvenbergen, I. Stassen, E. Gobechiya, Y. Zhang, K. Markey, D.E. De Vos, C. Kirschhock, B. Champagne, T. Verbiest, M. A. van der Veen, *Chem. Mater.* **2016**, *28*, 3203-3209.
[54] P. Yang, X. He, M. X. Li, Q. Ye, J. Z. Ge, Z. X. Wang, S. R. Zhu, M. Shao, H. L. Cai, *J. Mater. Chem.* **2012**, *22*, 2398-2400.
[55] Y. Wang, Y. X. Che, J. M. Zheng, *Inorg. Chem. Commun.* **2012**, *21*, 69-71
[56] M. Maczka, A. Gagor, N. L. M. Costa, W. Paraguassu, A. Sieradzkic, A. Pikul *J. Mater. Chem. C*, **2016**, *4*, 3185-3194.
[57] K. S. Asha, M. Makkitaya, A. Sirohi, L. Yadav, G. Sheetb, S. Mandal, *CrystEngComm.* **2016**, *18*, 1046-1053.
[58] M. Ptak, M. Maczka, A. Gagor, A. Sieradzki, A. Stroppa, D. Di Sante, J. M. Perez-Matoe, L. Macalik *Dalton Trans.* **2016**, *45*, 2574-2583.
[59] J. X. Gao, J. B. Xiong, Q. Xu, Y. H. Tan, Y. Liu, H. R. Wen, Y. Z. Tang *Cryst. Growth Des.* **2016**, *16*, 1559-1564.
[60] Y. Tian, S. Shen, J. Cong, L. Yan, S. Wang, Y. Sun *J. Am. Chem. Soc.* **2016**, *138*, 782-785.
[61] A. K. Srivastava, P. Divya, B. Praveenkumar, R. Boomishankar *Chem. Mater.* **2015**, *27*, 5222-5229.
[62] D. S. Liu, Y. Sui, W. T. Chen, P. Feng *Cryst. Growth Des.* **2015**, *15*, 4020-4025.
[63] J. Yang, L. Zhou, J. Cheng, Z. Hu, C. Kuo, C. W. Pao, L. Jang, J. F. Lee, J. Dai, S. Zhang, S. Feng, P. Kong, Z. Yuan, J. Yuan, Y. Uwatoko, T. Liu, C. Jin, Y. Long *Inorg. Chem.* **2015**, *54*, 6433-6438.
[64] Q. Li, T. Wu, J. C. Lai, Z. L. Fan, W. Q. Zhang, G. F. Zhang, D. Cui, Z. W. Gao, *Eur. J. Inorg. Chem.* **2015**, *31*, 5281-5290.
[65] L. Yu, X. N. Hua, X. J. Jiang, L. Qin, X. Z. Yan, L. H. Luo, L. Han *Cryst. Growth Des.* **2015**, *15*, 687-694.
[66] H. R. Wen, T. T. Qi, S. J. Liu, C. M. Liu, Y. Z. Tang, J. L. Chen, *Polyhedron* **2015**, *85*, 894-899.
[67] W. W. Zhou, B. Wei, F. W. Wang, W. Y. Fang, D. F. Liu, Y. J. Wei, M. Xu, X. Zhao, W. Zhao *RSC Adv.* **2015**, *5*, 100956-100959,
[68] J. A. Hua, Y. Zhao, D. Zhao, Y. S. Kang, K. Chen, W. Y. Sun, *RSC Adv. 2015*, *5*, 43268-43278.
[69] L. Pan, G. Liu, H. Li, S. Meng, L. Han, J. Shang, B. Chen, A. E. Platero-Prats, W. Lu, X. Zou, R. W. Li *J. Am. Chem. Soc.* **2014**, *136*, 17477-17483.
[70] Y. Tian, A. Stroppa, Y. Chai, L. Yan, S. Wang, P. Barone, S. Picozzi, Y. Sun *Sci. Rep.* **2014**, *4*, 6062.
[71] A. K. Srivastava, B. Praveenkumar, I. K. Mahawar, P. Divya, S. Shalini, R. Boomishankar *Chem. Mater.* **2014**, *26*, 3811-3817.
[72] Y. H. Tan, Y. M. Yu, J. B. Xiong, J. X. Gao, Q. Xu, C. W. Fu, Y. Z. Tang, H. R. Wen *Polyhedron* **2014**, *70*, 47-51.
[73] J. L. Qi, S. L. Ni, Y. Q. Zheng, W. Xu, *Solid State Sci.* **2014**, *28*, 61-66.
[74] S. L. Ni, W. Xu, Y. Q. Zheng, *J. Coord. Chem.* **2014**, *13*, 2287-2300.
[75] M. Sanchez-Andujar, L. C. Gomez-Aguirre, B. Pato Doldan, S. Yanez-Vilar, R. Artiaga, A. L. Llamas-Saiz, R. S. Manna, F. Schnelle, M. Lang, F. Ritter, A. A. Haghighiradde, M. A. Senaris-Rodriguez *CrystEngComm*, **2014**,*16*, 3558-3566.
[76] L. Z. Chen, D. D. Huang, J. Z. Ge, F. M. Wang, *Inorg. Chim. Acta*, **2013**, *406*, 95-99.
[77] X. F. Wang, G. X. Liu, H. Zhou, *Inorg. Chim. Acta* **2013**, *406*, 223-229.
[78] W. Xu, J. L. Lin, *Z. Naturforsch. B Chem. Sci.*, **2013**, *68*, 877-884.
[79] X. Y. Dong, B. Li, B. B. Ma, S. J. Li, M. M. Dong, Y. Y. Zhu, S. Q. Zang, Y. Song, H. W. Hou, T.C.W. Mak *J. Am. Chem. Soc.* **2013**, *135*, 10214-10217.
[80] Y. Z. Tan, M. Zhou, J. Huang, Y. H. Tan, J. S. Wu, H. R. Wen *Inorg. Chem.* **2013**, *52*, 1679-1681.
[81] P. C. Guo, Z. Chu, X. M. Ren, W. H. Ning, W. Jin, *Dalton Trans.* **2013**, *42*, 6603-6610.
[82] C. Pan, J. P. Nan, X. L. Dong, X. M. Ren and W. Q. Jin, *J. Am. Chem. Soc.* **2011**, *133*, 12330-12333
[83] H. Zhou, G. X. Liu, X. F. Wang, Y. Wang *CrystEngComm* **2013**, *15*, 1377-1388.
[84] T. Liu, D. Luo, D. Xu, H. Zenga, Z. Lin *Dalton Trans.* **2013**, *42*, 368-371.
[85] D. Feng, Y. Che, J. Zheng *J. Rare Earths* **2012**, *30*, 798-801.
[86] J. Wang, J. Q. Tao, X. J. Xu, C. Y. Tan *Z. Anorg. Allg. Chem.* **2012**, *9*, 1261-1264.
[87] X. Q. Yao, M. D. Zhang, L. Qin, Y. Z. Li *Cryst. Growth Des.* **2012**, *7*, 3426-3435.
[88] C. Hou, Q. Liu, Y. Lu, T. A. Okamura, P. Wang, M. Chen, W. Y. Sun, *Microporous Mesoporous Mater.* **2012**, *152*, 96-103.
[89] L. Li, J. Ma, C. Song, T. Chen, Z. Sun, S. Wang, J. Luo, M. Hong, *Inorg. Chem.* **2012**, *51*, 2438-2442.
[90] S. Q. Guo, D. Tian, X. Zheng, H. Zhang *CrystEngComm* **2012**,*14*, 3177-3182.
[91] Z. Su, G.-C. Lv, J. Fan, G. X. Liu, W. Y. Sun, *Inorg. Chem. Commun.* **2012**, *15*, 317-320.
[92] G. X. Liu, H. Xu, H. Zhou, S. Nishihara, X. M. Ren *CrystEngComm* **2012**, *14*, 1856-1864.
[93] D. Di Sante, A. Stroppa, P. Jain, S. Picozzi, *J. Am. Chem. Soc.* **2013**, *135*, 18126-18130.
[94] A. Stroppa, P. Jain, P. Barone, M. Marsman, J.M. Perez-Mato, A.K. Cheetham, H. W. Kroto, S. Picozzi *Angew. Chem. Int.* **2011**, *50*, 5847-5850.
[95] R.I. Thomson, P. Jain, A.K. Cheetham, M.A. Carpenter *Phys. Rev. B* **2012**, *86*, 214304.
[96] R. Yadav, D. Swain, H.L. Bhat, S. Elizabeth, *J. Appl. Phys.* **2016**, *119*, 064103.

[97] D. W. Fu, W. Zhang, H. L. Cai, Y. Zhang, J. Z. Ge, R. G. Xiong, S.D. Huang, T. Nakamura, *Angew. Chem. Int. Ed.* **2011**, *50*, 11947-11951.

[98] G. C. Xu, X. M. Ma, L. Zhang, Z. M. Wang, S. Gao *J. Am. Chem. Soc.* **2010**, *132*, 9588-9590.

[99] L. Wen, L. Zhou, B. Zhang, X. Meng, H. Qu, D. Li *J. Mater. Chem.* **2012**, *22*, 22603-22609.

[100] S. Horiuchi, Y. Tokura *Nat. Mater.* **2008**, *7,* 357-366.

[101] C. M. Foster, G.R. Bai, R. Csencsits, J. Vetrone, R. Jammy, L. A. Wills, E. Carr, J. Amano *J. Appl. Phys.* **1997**, *81*, 2349-2357.

[102] K. Asadi, M. Li, P. W.M. Blom, M. Kemerink, D. M. de Leeuw *Materials Today* **2011**, *14*, 592-599.

[103] D. W. Fu, H. L. Cai, Y. Liu, Q. Ye, W. Zhang, Y. Zhang, X. Y. Chen, G. Giovannetti, M. Capone, J. Li, R. G. Xiong *Science* **2013**, *339*, 425-428.

[104] P. Jain, N.S. Dalal, B.H. Toby, H.W. Kroto, A.K. Cheetham *J. Am. Chem. Soc.* **2008**, *130*, 10450-10451.

[105] P. Jain, V. Ramachandran, R.J. Clark, H. D. Zhou, B.H. Toby, N.S. Dalal, H.W. Kroto, A.K. Cheetham *J. Am. Chem. Soc.* **2009**, *131*, 13625-13627.

[106] M. Sanchez-Andujar, S. Presedo, S. Yanez-Vilar, S. Catro-Garcia, J.Shamir, M.A. Senaris-Rodriguez *Inorg. Chem*. **2010**, *49*, 1510–1516.

[107] M. Simenas, S. Balciunas, M. Maczka,J. Banys, E. Tornau *Phys. Chem. Chem. Phys*. **2016**, 18, 18528-18535.

[108] T. Besara, P. Jain, N.S. Dalal, P.L. Kuhns, A.P. Reyes, H.W. Kroto, A.K. Cheetham *PNAS* **2011**, *108*, 6828-6832.

[109] M. Šimėnas, A. Ciupa, M. Mączka, A. Pöppl, J. Banys *J. Phys. Chem. C* **2015**, 119, 24522−24528

[110] M. Maczka, M. Ptak, S. Kojima, *Appl. Phys. Lett.* **2014**, *104*, 222903.

[111] D. Zhao, I. Katsouras, K. Asadi, P. W. M. Blom, D. M. de Leeuw *Phys. Rev. B* **2015**, *92*, 214115.

[112] A. Stroppa, P. Barone, P. Jain, J.M. Perez-Mato, S. Picozzi *Adv. Mater.* **2013**, *25*, 2284-2290.

[113] W. Wang, L. -Q. Yan, J. -Z. Cong, Y. -L. Zhao, F. Wang, S. -P. Shen, T. Zou, D. Zhang, S. -G. Wang, X. -F. Han, Y. Sun *Sci. Rep.* **2013**, *3*, 2024.

[114] O. Shekhah, J. Liu, R. A. Fischer, Ch. Wöll *Chem. Soc. Rev*. **2011**, *40*, 1081-1106.

[115] P. Falcaro, R. Ricco, C.M. Doherty, K. Liang, A. J. Hill, M. J. Styles *Chem. Soc. Rev*. **2014**, 43, 5513—5560.

[116] I. Stassen, M. Styles, G. Grenci, H. Van Gorp, W. Vanderlinden, S. De Feyter, P. Falcaro, D. De Vos, P. Vereecken, R. Ameloot *Nat. Mater.* **2016**, *15*, 304–310.

[117] J. Roscow, Y. Zhang, J. Taylor, C.R. Bowen *Eur. Phys. J. Special Topics* **2015**, *224*, 2949–2966.

[118] R. Ramesh *Nature* **2009**, *461*, 1218-1219.

[119] G. Rogez, N. Viart, M. Drillon *Angew. Chem. Int. Ed.* **2010**, *49*, 1921 – 1923.

[120] Y. Tian, W. Wang, Y. Chai, J. Cong, S. Shen, L. Yan, S. Wang, X. Han, Y. Sun *Phys. Rev. Lett.* **2014,** 112, 017202.

[121] Y. Tian, J. Cong, S. Shen, Y. Chai, L. Yan, S. Wang, Y. Sun *Phys. Status Solidi RRL* **2014,** 8, 91–94.

[122] B. Pato-Doldan, M. Sanchez-Andujar, L.C. Gomez-Aguirre, S. Yanez-Vilar, J. Lopez-Beceiro, C. Gracia-Fernandez, A. A. Haghighirad, F. Ritter, S. Castro-Garcıa *Phys. Chem. Chem. Phys*. **2012**, 14, 8498–8501.

[123] M. Maczka, A. Pietraszko, B. Macalik, K. Hermanowicz *Inorg. Chem.* **2014**, 53, 787-794.

[124] G.-C. Xu, W. Zhang, X.-M. Ma, Y.-H. Chen, L. Zhang, H.-L. Cai, Z.-M. Wang, R.-G. Xiong, S. Gao *J. Am. Chem. Soc.* **2011**, 133, 14948–14951.

[125] Y. Tian, A. Stroppa, Y.-S. Chai, P. Barone, M. Perez-Mato, S. Picozzi, Y. Sun *Phys. Status Solidi RRL* **2015**, 9, 62-67.

[126] M. Maczka, A. Ciupa, A. Gagor, A. Sieradzki, A. Pikul, M. Ptak J. *Mater. Chem. C* **2016**, 1186-1193.

[127] M. Maczka, A. Sieradzki, B. Bondzior, P. Deren, J. Hanuza, K, Hermanowicz *J. Mater. Chem. C* **2015**, 9337-9345.

[128] M. Maczka, A. Gagor, B. Macalik, A. Pikul, M. Ptak, J. Hanuza *Inorg. Chem.* **2014**, 457-467.

[129] H. Cui, Z. Wang, K. Takahashi, Y. Okano, H. Kobayashi, A. Kobayashi J. Am. Chem. Soc. 2006, 128, 15074-15075.

[130] H.-X. Zhao, X.-J. Kong, H. Li, Y.-C. Jin Proc. Nat. Ac. Sci. 2011, 108, 3481-3486.

Entry for the Table of Contents (Please choose one layout)

MICROREVIEW

Ferroelectric metal organic frameworks are emerging as an exciting field of research, and have witnessed a great progress in the last decade. In this contribution we briefly discuss ferroelectricity and its means of demonstration. We critically discuss different mechanisms leading to ferroelectricity as well as the state-of-the-art ferroelectric metal-organic frameworks.

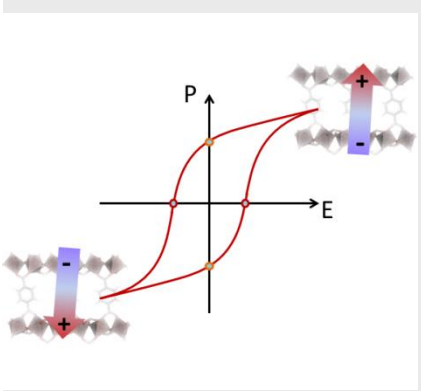

Ferroelectric metal-organic frameworks*

Kamal Asadi, Monique A. van der Veen**

Page No. – Page No.

Ferroelectricity in metal-organic frameworks: characterization and mechanisms

*one or two words that highlight the emphasis of the paper or the field of the study